

# Electric field reconstruction in the image plane of a high-contrast coronagraph using a set of pinholes around the Lyot plane

Amir Give'on<sup>a</sup>, Stuart Shaklan<sup>a</sup>, Brian Kern<sup>a</sup>, Charley Noecker<sup>a</sup>, Steve Kendrick<sup>b</sup>, Kent Wallace<sup>a</sup>

<sup>a</sup>Jet Propulsion Laboratory, California Institute of Technology, Pasadena, California, USA;

<sup>b</sup>Ball Aerospace & Technologies Corp., Boulder CO, USA

## ABSTRACT

In a setup similar to the self coherent camera, we have added a set of pinholes in the diffraction ring of the Lyot plane in a high-contrast stellar Lyot coronagraph. We describe a novel complex electric field reconstruction from image plane intensity measurements consisting of light in the coronagraph's dark hole interfering with light from the pinholes. The image plane field is modified by letting light through one pinhole at a time. In addition to estimation of the field at the science camera, this method allows for self-calibration of the probes by letting light through the pinholes in various permutations while blocking the main Lyot opening. We present results of estimation and calibration from the High Contrast Imaging Testbed along with a comparison to the pair-wise deformable mirror diversity based estimation technique. Tests are carried out in narrow-band light and over a composite 10% bandpass.

**Keywords:** high contrast imaging, coronagraphs

## 1. INTRODUCTION

This paper follows a report which discussed the completion of the Advanced Speckle Sensing for Internal Coronagraphs (ASSIC) proposal, funded under the 2009 Technology Development for Exoplanet Missions Initiative. The ASSIC report was a laboratory verification of the consistency of dark-hole contrast estimation in a band-limited coronagraph to better than  $2 \times 10^{-9}$  using two independent estimation approaches: deformable mirror phase diversity (PD), and reference beams formed using pinholes adjacent to the Lyot stop (PH). This was achieved in broad band light having a 10% fractional bandwidth over a region  $5 \times 18 \lambda/D$  wide. '

It has been proven that it is possible to estimate the complex field in the image plane and to control scattered light to levels better than  $10^{-9}$ , in broadband light, over a region several  $\lambda/D$  wide.<sup>1</sup> The estimation technique was based on the phase diversity generated with patterns commanded on the Deformable Mirror (DM). In theory, as long as one has a means of accurately estimating the contrast, then with enough degrees of freedom and adequate calibration of the DM, the contrast can be controlled to arbitrarily deep levels. But in reality, for a number of reasons (e.g., number of degrees of freedom, stability) the convergence bottoms out and speckles remain at levels that can mask the presence of a planet.

There are several approaches that may allow the speckles to be identified and subtracted from the image in space applications such as roll subtraction<sup>2</sup> and spectral deconvolution.<sup>3</sup> In both the cases of roll subtraction and spectral deconvolution, however; the achromatic nature of the speckles where planets would appear in the image plane prohibit these methods from being effective for Earth-like planet detection applications. We have found that spectral deconvolution in these conditions is effective if the location of the planet is known.<sup>4</sup>

The purpose of the Advanced Speckle Sensing for Internal Coronagraphs (ASSIC) TDEM was to develop an independent means of estimating the complex electric field to confirm the accuracy of the phase diversity estimation. We developed an interferometric approach that is a variant of the self-coherent camera introduced by Baudoz.<sup>5-7</sup> We place pinholes just outside the edge of the Lyot stop, in the region where the diffracted light is blocked. The pinholes are opened one or two at a time to generate tilted wavefronts in the image plane. These wavefronts serve as reference beams that interfere with the light that passes through the center of the Lyot stop. A mathematical treatment similar to that of PD provides an estimate of the complex field in the image. The

main difference between PH and PD estimation is that with PD we difference pairs of images that introduce opposing changes in the image plane, whereas with PH we difference each diversity image with the non-diversity image.

There are two important advantages to the PH approach. First, except for a sliding mask that blocks and unblocks the pinholes, there are no moving parts. Whereas PD requires moving the hysteretic, non-linear DM, the PH approach simply requires exposing the image plane to light that passes through the pinholes. Second, the additive electric field from the pinholes can be treated without approximation in the image plane. This is not the case for PD, which modifies the phase of the field in the pupil but does not exactly add field ( $e^{i\phi}$  is treated as  $1 + i\phi$ ). This can be a limiting factor because our wavefront control technique (Electric Field Conjugation, or EFC<sup>8</sup>) does not flatten the phase in the pupil, it finds the phase that removes light from the dark hole region. Thus  $\phi$  is not necessarily small.

## 2. PINHOLE ESTIMATION TECHNIQUE

The experiment approach for PH was first described by Noecker et al.<sup>10</sup> In a linear band-limited Lyot coronagraph configuration, we place four pinholes in locations that allow reasonably robust solutions for the speckle field with a good distribution of phases at each pixel.

Given a complex electric field in the final image plane of a Lyot coronagraph,  $E_0$  and the ability to independently let light through four different pinholes on the side of the main opening of the Lyot stop, we can model the intensity of light in the image plane for five different cases as

$$\begin{aligned}
 I_0 &= |E_0|^2 + I_{inc} \\
 I_{oa} &= |E_0 + E_a|^2 + I_{inc} \\
 I_{ob} &= |E_0 + E_b|^2 + I_{inc} \\
 I_{oc} &= |E_0 + E_c|^2 + I_{inc} \\
 I_{od} &= |E_0 + E_d|^2 + I_{inc}
 \end{aligned} \tag{1}$$

where  $I_0$  is the intensity of light for the case where all 4 pinholes are blocked and light only goes through the main opening of the Lyot mask.  $I_{oa}$ ,  $I_{ob}$ ,  $I_{oc}$  and  $I_{od}$  represent the intensity of light for the four cases where the main opening of the Lyot mask is open and one of the pinholes, a, b, c or d, respectively, is open.  $E_a$ ,  $E_b$ ,  $E_c$  and  $E_d$  are the electric fields in the image plane due to the light going through each of the pinholes and reaching the image plane, respectively, and  $I_{inc}$  is the incoherent light in the system that goes through the main opening of the Lyot stop. Unlike the pair-wise estimation technique used with the deformable mirror, these set of equations are exact and not an approximation because of the linearity of the optical system. Given a model description of the optical path to each of the pinholes, their location and size, it is possible to model the expected electric field of each of the pinholes and then solve for  $E_0$  using the following relationship with measurements of the intensity of light in the five cases above.

$$\begin{bmatrix} \Re\{E_0\} \\ \Im\{E_0\} \end{bmatrix} = \frac{1}{2} \begin{bmatrix} -\Im\{E_a\} & \Re\{E_a\} \\ -\Im\{E_b\} & \Re\{E_b\} \\ -\Im\{E_c\} & \Re\{E_c\} \\ -\Im\{E_d\} & \Re\{E_d\} \end{bmatrix} \begin{bmatrix} I_{oa} - I_0 - |E_a|^2 \\ I_{ob} - I_0 - |E_b|^2 \\ I_{oc} - I_0 - |E_c|^2 \\ I_{od} - I_0 - |E_d|^2 \end{bmatrix} \tag{2}$$

Figure 1 shows the arrangement of pinholes around the outside of the Lyot stop opening. Solving for the real and imaginary parts of  $E_0$  involves inversion of the matrix in equation 2 for each of the pixels in the region of interest (each pixel has a unique matrix to invert) using the pseudo inverse since the matrix is over-determined (4 rows by 2 columns). We derived the configuration for the 4 pinholes based on a model for this matrix for all the pixels in the desired dark zone. The linear (along the y axis) symmetry of the occulter and a specification of 300 microns for the diameter of the pinholes, both defined the horizontal distance of the center of the pinholes from

the location in the Lyot plane where the electric field amplitude flips its sign. For a given distribution of the 4 pinholes, the condition number of the 4x2 matrix for each pixel represents the expected degree of independence between the different measurements. If all reference beams have similar optical phase at a particular pixel, there will be a high degeneracy between the 4 measurements in that pixel and thus a poor solution (a large condition number). In other words, a large condition number (ratio between the smallest and the largest singular values in the matrix) implies a large amplification of noise after inversion. In our observation scenario, 5 images are taken (see equation 1): one with the speckles and no reference beam; and four with speckles and each of the 4 reference beams in turn (each reference beam is engaged by uncovering the corresponding pinhole). We explored a range of pinhole configurations with a simple line search (and a slightly larger dark zone than the goal) and found one configuration (see figure 1) with a small maximum condition number for pixels in the dark hole region. The value “3.17” means that the errors in the system (from measurement) will be amplified by  $\sqrt{3.17}$  when applying the inversion. We do not claim that the pinhole locations we found are globally optimal, but they are adequate for our experiments.

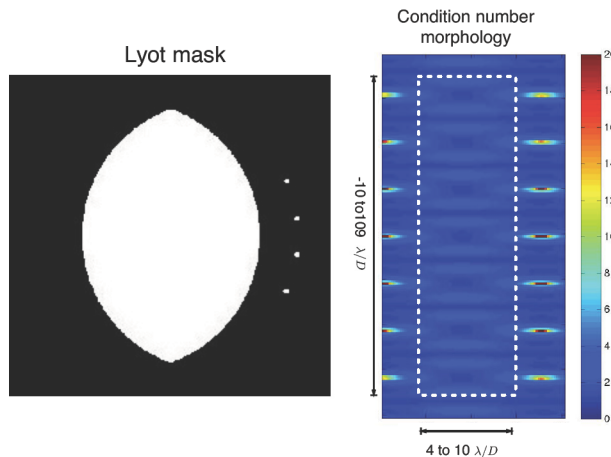


Figure 1. Pinholes adjacent to Lyot stop, and quality of solution. Left: Arrangement of pinholes around the outside of the central opening of the Lyot stop. The Football is the traditional opening in the Lyot mask, where the planet light and speckles pass through the Lyot stop. This one is tailored for a linear band-limited mask and has  $e=0.34$ . The edge radius of curvature is 12.4 mm. The four pinholes are arranged on an arc at right. Right: the condition number at each pixel for a best solution for PH diversity-derived speckle fields. XY axes are equivalent sky angles in units of  $\lambda/D$ . Within the range from 4 to 10  $\lambda/D$  horizontally and -10 to 10  $\lambda/D$  vertically, the minimum condition number is 1 (ideal), and the maximum is 3.17.

We have designed and implemented a shutter mechanism for selecting which pinholes are open to illuminate the focal plane (figure 2). With all pinholes blocked and the main opening of the Lyot stop unblocked, we can take science data, and calibrate the speckle intensity with no reference beams. This state is also used for DM Phase Diversity (PD). Using each pinhole unblocked one at a time with the main opening of the Lyot stop unblocked, we can capture interference images to support a solution for the speckle fields.

With our PH-derived estimate of the speckle fields, we may choose to correct the speckles using the DM (correction mode) or simply to estimate and subtract the speckle intensity from the science data (detection mode).

Currently our method uses 4 pinholes, and thus 5 images taken in succession. In theory, the minimum number of equations is 2 and it is possible to solve them with just two pinhole measurements. However, the periodicity of the diversity in the image plane from the tilted wavefronts originating at the pinholes creates regions of low diversity (large condition number for the 4x2 matrix in equation 2). For planet searches in a large dark hole, it is likely that at least 3 pinholes are required. For characterization of planets in a known region of the dark hole, two pinholes can be selected to give adequate diversity.

For these experiments at HCIT, we used five 2% filters, centered at 768, 784, 800, 816 and 832 nm, covering

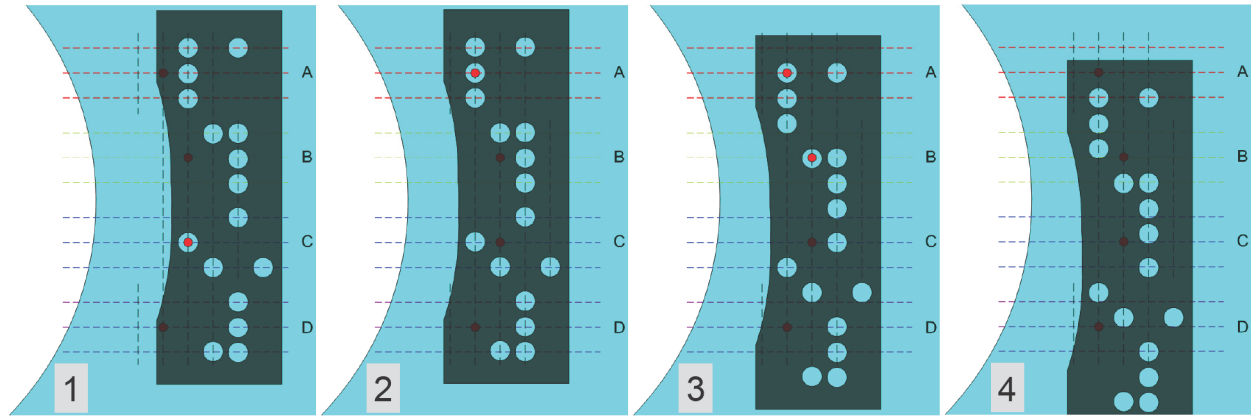


Figure 2. Sliding-mask shutter mechanism. With 3 vertical positions and 4 horizontal, the dark gray sliding mask offers 12 possible combinations of open/closed pinholes. Shown here are 4 of the 11 states we actually need: (1) only pinhole C is open; (2) only pinhole A is open; (3) pinholes A and B are both open; and (4) none of the pinholes are open.

together a 10% band. Figure 3 shows the different measurements at different wavelengths. Each row in the figure represents the 5 measurements that are modeled in equation 1.

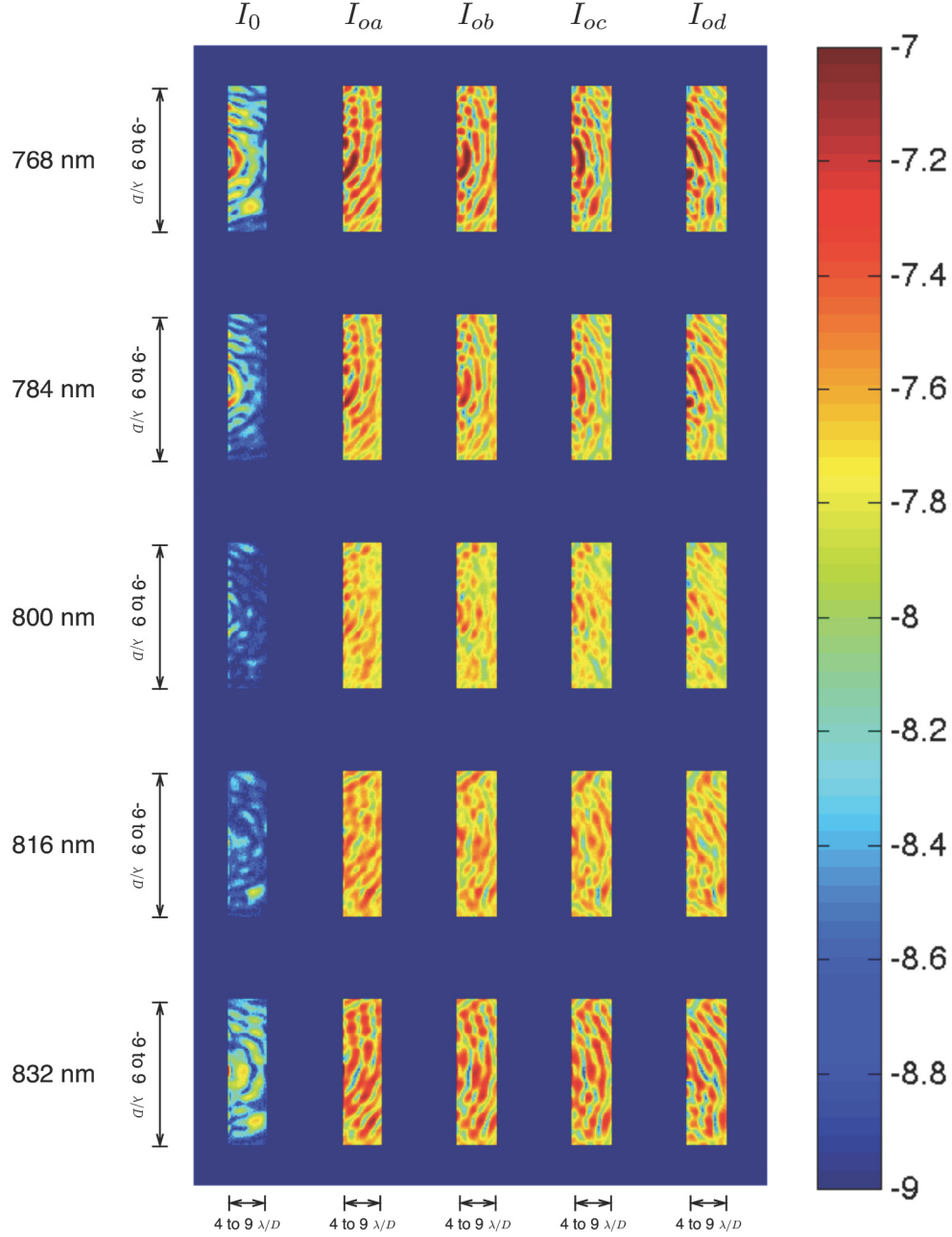


Figure 3. Estimation measurements. With 5 different wavelength filters and 4 diversity images, this figure shows all the measurements taken following equation 1. EFC was used to drive the average contrast of the 5 bands (the left most column) slightly below  $10^{-8}$ . Then, the shutter mechanism described in figure 2 was used to take the 4 diversity intensity measurements in each of the bands (the other 4 columns). As seen in the figure, the resulting diversity images intensity is slightly over  $10^{-8}$ .

The estimation process was done in two steps: "model-based" and "measurement-based calibration". As seen in equation 2, in order to solve for  $E_0$  at each location in the image plane, one needs an estimate of the EF in the image plane at those locations for each of the pinholes. The first step was to model the EF in the final image plane due to the light going through each pinhole based on all *a priori* knowledge (complex EF in the entrance pupil from phase retrieval, propagation through the occulter model and finally passage through the best known estimate of the location and size of the pinholes from an image of the Lyot stop to focus at the final image plane

where intensity measurements are taken). This gives an initial estimate for  $E_a$ ,  $E_b$ ,  $E_c$  and  $E_d$ .

### 3. MODEL CALIBRATION

The system at hand also allows us to block the Lyot stop main opening and independently let light through the pinholes, one at a time or in pairs. These measurements can be used to better calibrate the model of the electric field of the light going through the pinholes that was used in solving for  $E_0$  in equation 2. Blocking the Lyot stop and letting light through each of the pinholes independently gives the first 4 measurements that determines the amplitude of the electric field at each pixel in the image plane due to each of the pinholes (by taking the square root of the measured intensity) as shown in the equation set 3:

$$\begin{aligned} I_a &= |E_a|^2 \\ I_b &= |E_b|^2 \\ I_c &= |E_c|^2 \\ I_d &= |E_d|^2 \end{aligned} \tag{3}$$

Figure 4, below, shows the intensity measurements of these 4 cases for one of the particular band filters. In this case we are showing the measurements at the 800 nm centered filter.

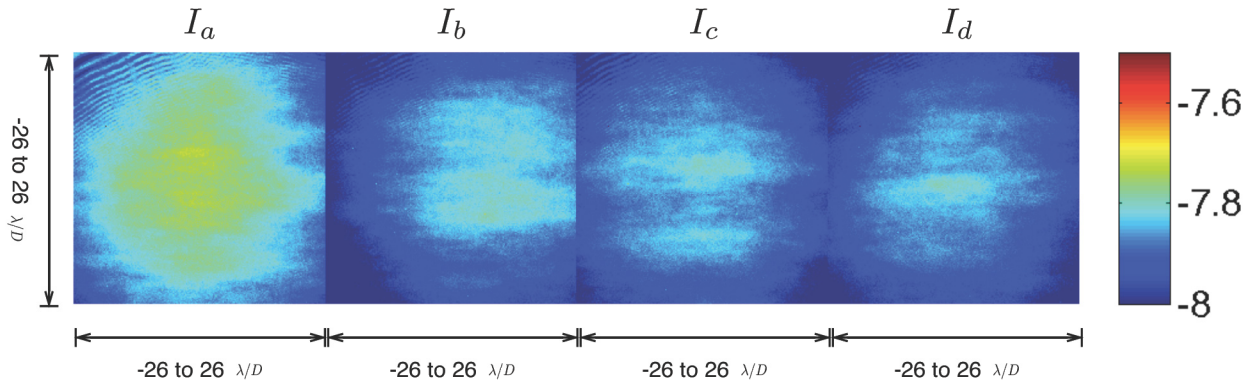


Figure 4. Calibration images: single pinholes. These are the intensity images for the calibration of the EF due to the pinholes. In these 4 cases, the main opening of the Lyot stop is blocked and one pinhole at a time is exposed at each time according to equation 3. We believe the variation in intensity between the 4 measurements comes from misalignment of the shutter mechanism with the locations of the pinholes. Nevertheless, these measurements were used to determine the amplitude of the EF due to each of the pinholes.

The pinholes locations (relative on the Lyot mask) and their diameter were chosen such that the average contrast in the “dark zone” region would be roughly  $10^{-8}$ . As seen in the 4 images above, we have succeeded to do so. We believe the global variations (Ranging from  $10^{-8}$  to  $3 * 10^{-8}$ ) between the pinholes (even though the design was such that they should produce the same intensity levels) is due to misalignment of the sliding mask that covers the different pinholes (see figure 2). We cannot fully explain the non uniformity of the intensity morphology of each of the measurements. It is possible this is due to non-modeled variations in phase across the pinholes at the Lyot plane.

In order to estimate the phase of the EF of the light going through the pinholes, the next measurements interfered the lights from two different pinholes each time, per wavelength filter. The model for these measurements is shown in the equation set 4:

$$\begin{aligned}
I_{ab} &= |E_a + E_b|^2 \\
I_{ac} &= |E_a + E_c|^2 \\
I_{ad} &= |E_a + E_d|^2 \\
I_{bc} &= |E_b + E_c|^2 \\
I_{bd} &= |E_b + E_d|^2 \\
I_{cd} &= |E_c + E_d|^2
\end{aligned} \tag{4}$$

As seen in this model, it is only possible to find the relative phase difference between the effects of each pinhole rather than the absolute phase (or relative to the phase of the light through the main opening of the Lyot mask). Figure 5 shows the intensity measurements of the interference of the EF's from two pinholes at a time using the 800 nm centered filter:

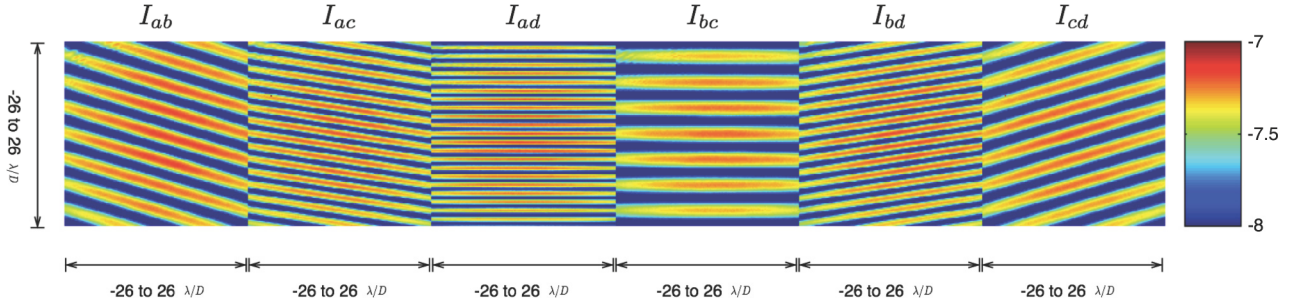


Figure 5. Calibration images: pairs of pinholes. These are the intensity images for the calibration of the EF due to the pinholes. In these 6 cases, the main opening of the Lyot stop is blocked and two pinholes are exposed at each time according to equation 4 (last 6 lines).

The second step of the estimation process uses these 10 measurements (figure 4 and figure 5). The first 4 (seen in figure 4) are used to determine the amplitude of  $E_a$ ,  $E_b$ ,  $E_c$  and  $E_d$  with a simple square root operation. The 6 measurements shown in figure 5 were then used to estimate the three phase differences, per pixel, for  $E_a$ ,  $E_b$ ,  $E_c$  and  $E_d$  using least squares minimization between the RHS and the LHS of the model equations (taking the LHS as the measured intensity). In order to compare to other estimation techniques or to use the estimate for correction (such as in EFC), the relative phase between the phase due to the pinholes and due to the light that goes through the main opening of the Lyot, must be determined. One way to do this is to use DM-diversity estimation before and after letting light through the pinhole (and the main opening of the Lyot stop). Another way is to use the same phase conventions used in the phase diversity using the DM to propagate the light through one of the pinholes (in modeling), as was done in the first stage of the estimation. That is, use the best knowledge of the system to determine the phase due to one of the pinholes and then use the calibration to determine the relative phase between the EF's due to the other pinholes.

The internal agreement (or disagreement) between the estimate for the complex EF of  $E_a$ ,  $E_b$ ,  $E_c$  and  $E_d$  and the measured intensities through the model in equation 4 could be expressed in RMS, taking into account the degrees of freedom in the system. The degrees of freedom are the number of measurements minus the number of fit parameters. In the first case (pure model), there are 10 measurements and no fit parameters (DOF=10). In the second step, there are 10 measurements and 7 fit parameters (4 amplitudes and 3 relative phases), giving DOF=3. Figure 6 shows the distribution of RMS of the difference, taking into account the DOF in both cases. With an average intensity over the dark zone of  $2.9 * 10^{-8}$  for the measurements, the average disagreement over all pixels and all filters dropped from 56% to 7% by using the calibration measurements.

Another way of depicting the advantage of using the calibration measurements with the parameter fitting through the model for these measurements (i.e. an estimate that agrees with the measurements) is to look at the

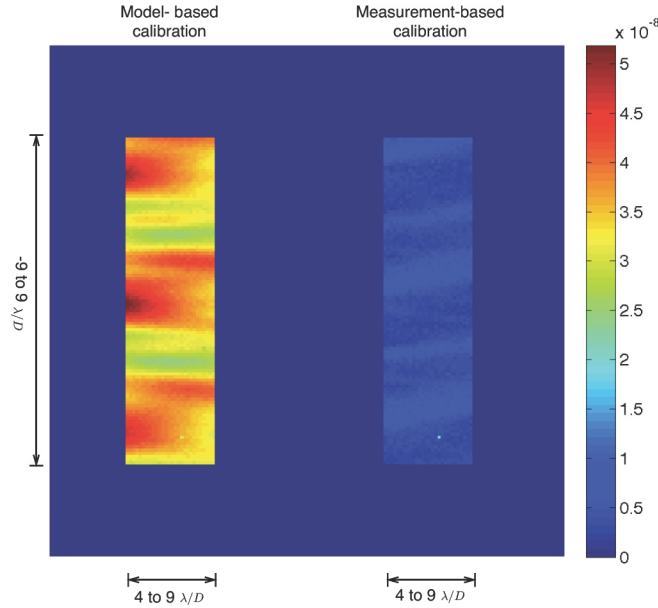


Figure 6. Internal agreement between measurements and model. The two images show the RMS of the difference between the measurements and the model (with the estimates) in both cases. First case is purely based on model and the second case is based on the calibration images. The disagreement dropped from 56% to 7% by using the calibration images.

RMS of the difference between the measurements and the model per wavelength filter, i.e. the incoherent light  $I_{inc}$ . Figure 7 shows the measured intensity for each of the filters along side the estimated coherent intensity (from squaring the estimated coherent EF) and the RMS of the difference between them, for both the model based case and the calibration based case. As seen in the figure, the effect of the calibration based on the measured intensities was to reduce the estimated incoherent component. The RMS of the difference for the model based for the five wavelength filters (third column) is 71%, 78%, 92%, 70% and 60%, respectively. The RMS of the difference dropped to 27%, 33%, 49%, 44% and 28%, respectively, after using the calibrated images.

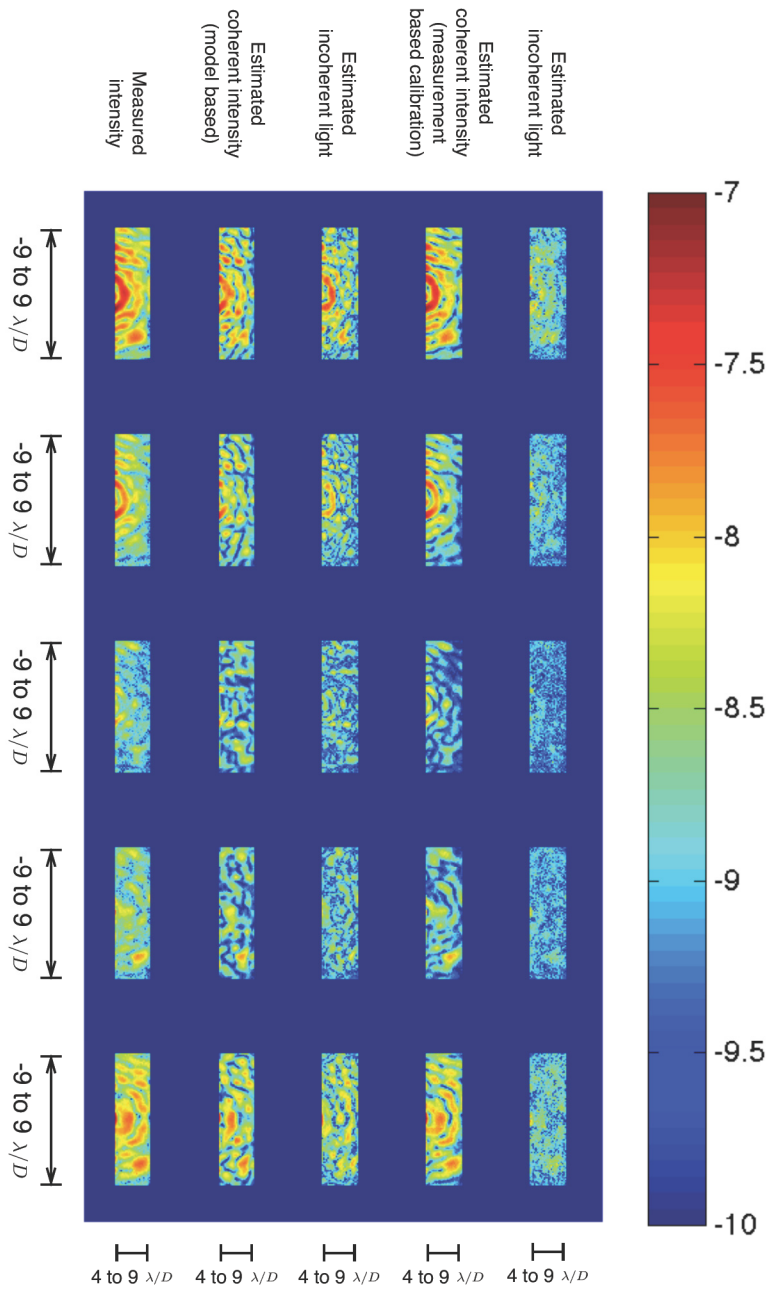


Figure 7. Estimation error. The figure shows the estimation of the intensities that were measured from the estimation of the complex EF  $E_0$  in each of the wavelength bands. The RMS of the difference for the model based for the five wavelength filters (third column) is 71%, 78%, 92%, 70% and 60%, respectively. The RMS of the difference dropped to 27%, 33%, 49%, 44% and 28%, respectively, after using the calibrated images.

#### 4. DM DIVERSITY VERSUS PINHOLES DIVERSITY ESTIMATIONS

The pair-wise DM diversity estimation technique has been used for many years now to produce the best high contrast imaging results in different labs.<sup>1</sup> There are two conceivable ways to compare the pairwise estimation technique to the pinholes based diversity presented here. One is indirectly by using them both in a closed loop system alongside correction, and compare the resulting contrast. Since the correction involves using the DM which could have its own modeling errors, we decided to use the more direct method and compare the estimation results of the two methods for the same system configuration.

In order to compare the two estimation processes, the system was driven to a high contrast state (average of  $3 * 10^{-9}$  across 10% light band) within the region discussed throughout this paper. At this configuration, the pinholes estimate was used first and then the DM estimation (pairwise) was used. Both were completed within 3 hours which in past experience with HCIT shows to be well within stability criteria for this comparison at this contrast level.

Figure 8 shows the coherent intensity agreement between the two methods. Both methods were used to get an estimate of the coherent EF in the 5 wavelength bands. The absolute valued squared of the estimated EF in the 5 bands were low pass filtered to  $0.5\lambda/D$  prior to analysis in order to reduce white noise (e.g., CCD read noise and Poisson noise) from the measurements. The RMS of the difference of intensities across the 5 bands is 11% of the average intensity of the two methods.

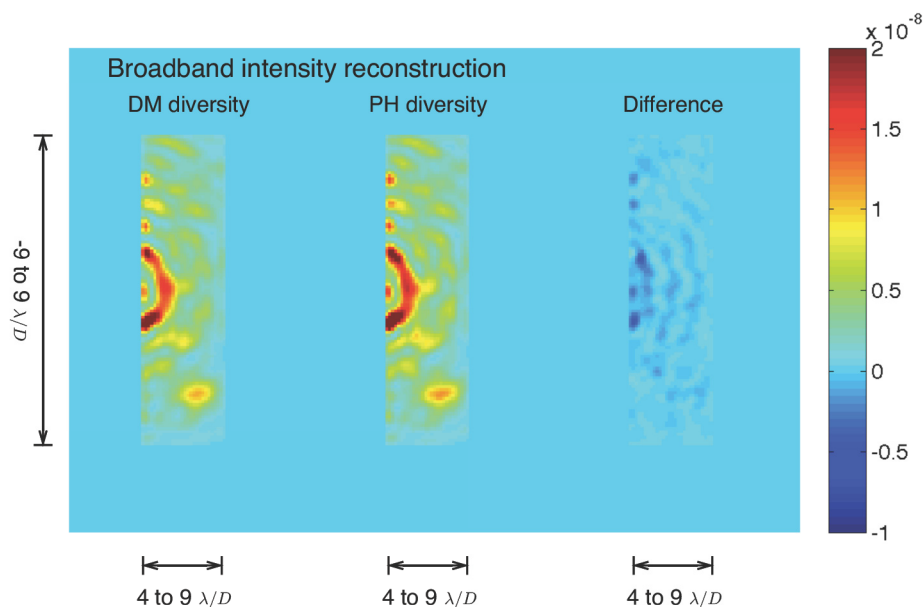


Figure 8. Direct comparison of the two methods' intensity estimates. The left figures shows the composite intensity of the estimated field from DM diversity from the 5 bands. The middle figure shows the composite intensity of the estimated field from the pinhole diversity from the 5 bands. The right figure shows the average difference between the intensities in the 5 bands of the two methods. The RMS of the difference of intensities across the 5 bands is 11% of the average intensity of the two methods.

While the intensities can be added to create an estimate of the broadband intensity image, phases do not add. Figure 9 shows the comparison between the two methods and their resulting phases in all 5 bands.

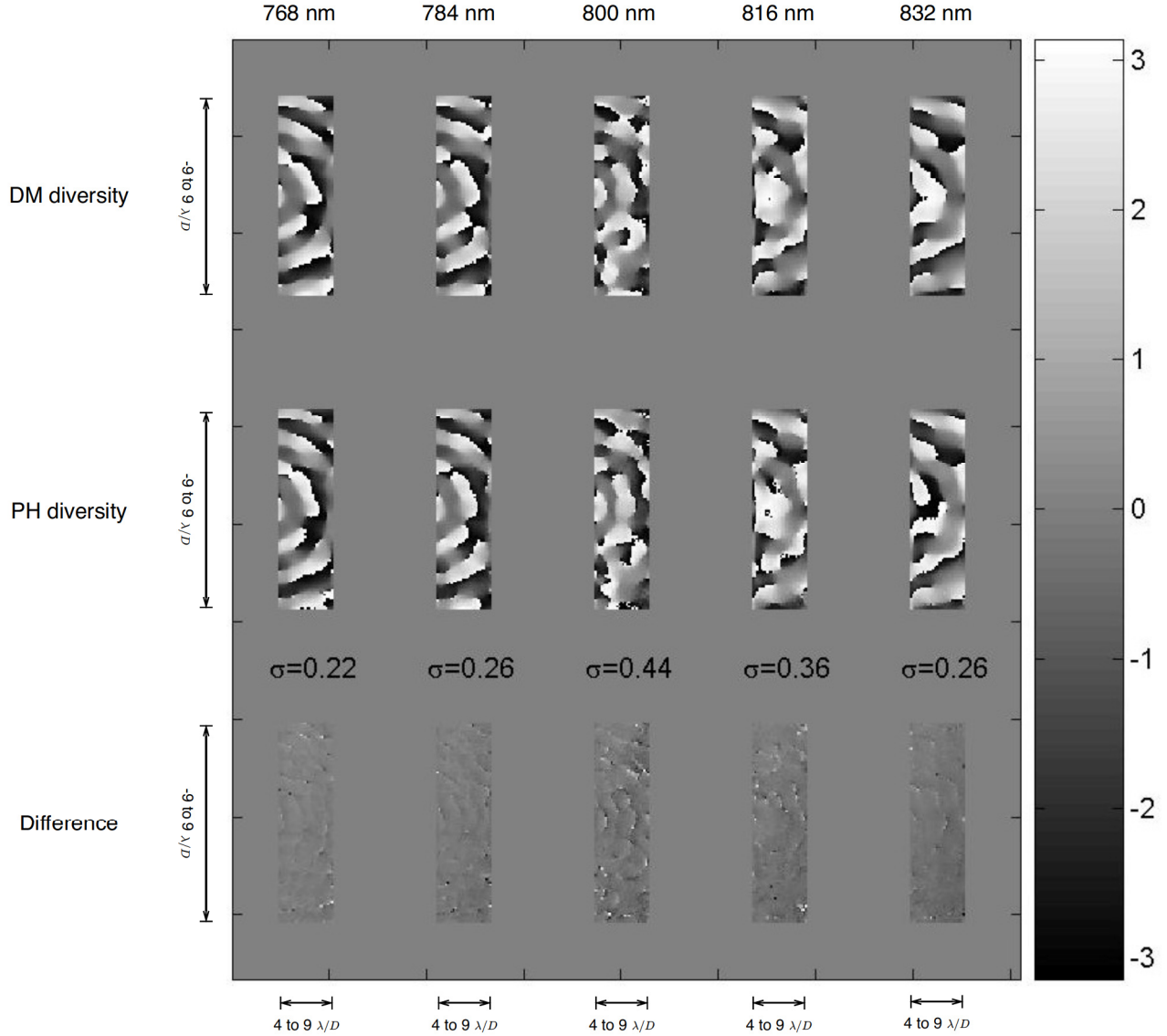


Figure 9. Phase comparison between the two estimation methods. This figure shows the comparison between the DM diversity based solution to the pinholes diversity based solution. The first row shows the phase of the EF in the image plane for the case of using DM diversity in the 5 different bands. The second row shows the phase of the solution obtained using the pinhole diversity based method. Their difference is shown in the bottom row. The average sigma of the RMS of the difference is 0.31 radians.

## 5. SUMMARY AND FUTURE WORK

This paper presented the implementation and initial results from adding a set of pinholes in the diffraction ring of the Lyot plane in a high-contrast stellar Lyot coronagraph in order to estimate the complex EF in the image plane. We describe the theory behind the estimation process, the mechanism used to uncover the pinholes as needed and a novel calibration process to get a better model for the diversity probes themselves. We presented results of estimation and calibration from the High Contrast Imaging Testbed (HCIT) along with a comparison to the pair-wise deformable mirror diversity based estimation technique. Tests were carried out in narrow-band light and over a composite 10% bandpass in a region  $5 \times 18 \lambda/D$  wide ( $4$  to  $9 \lambda/D$  in  $x$  and  $-9$  to  $9 \lambda/D$  in  $y$ ) at an average contrast level of  $3 \times 10^{-9}$ .

The estimation process is very similar to that of the pairwise DM diversity. We have pointed out a few differences and some advantages. The main advantage in the modeling of the measured intensity is that no approximations are needed. The greatest advantage pinholes diversity has over DM diversity is the ability to “turn off” the main beam (cover the main opening of the Lyot stop) and calibrate the probes. In this case, by measuring their intensity in the image plane and interfering them one against each other. We showed the calibration process and its results in improving the self consistency of the estimated probe complex EF with the measurements.

Future work consists of more comparisons between pinholes based estimation and the DM diversity based pair-wise estimation. Both directly compared but mostly indirectly through closed loop correction.

## ACKNOWLEDGMENTS

This work was carried out in part at the Jet Propulsion Laboratory, California Institute of Technology, under contract with the National Aeronautics and Space Administration. Copyright 2012. All rights reserved.

## REFERENCES

- [1] B. Kern, A. Kuhnert, & J. Trauger, Exoplanet Exploration Coronagraph Technology Milestone #2 Report, JPL Document D-60951, Aug 8, 2008.
- [2] J. Trauger & W. Traub, A laboratory demonstration of the capability to image an Earth-like extrasolar planet, *Nature* 446, 771-773 (2007).
- [3] W. Sparks and H. Ford, Imaging spectroscopy for extrasolar planet detection, *Ap. J.* 578, 543-564 (2002).
- [4] J. Krist, S. Shaklan, & M. Levine, Extraction of extrasolar planet spectra from realistically-simulated, wavefront-corrected coronagraph fields, *Proc. SPIE* 7010, 701044-1 (2008).
- [5] P. Baudoz et al, The self-coherent camera: a new tool for planet detection, *Proc. IAU Colloq.* 200, 553-558 (2005).
- [6] R. Galicher, P. Baudoz, & G. Rousset, Wavefront error correction and Earth-like planet detection by a self-coherent camera in space *A&A* 488, L9-L12 (2008).
- [7] R. Galicher et al, Self-coherent camera as a focal plane wavefront sensor: simulations, *A&A* 509, A31 (2010).
- [8] A. Give'on, et al, "Broadband wavefront correction algorithm for high-contrast imaging systems", *Proc. SPIE* 6691, 66910A (2007).
- [9] S. Kendrick et al, Technology Milestone White Paper Advanced Speckle Sensing for Internal Coronagraphs, JPL Document D-68673. Originally published April 29, 2011. Revised Nov. 28, 2011.
- [10] C. Noecker, et al, Advanced Speckle Sensing for Internal Coronagraphs, *Proc. SPIE* 8151, 81510I (2011).
- [11] J. Trauger et al, "A hybrid Lyot coronagraph for the direct imaging and spectroscopy of exoplanet systems: recent results and prospects", *Proc. SPIE* 8151, 81510G (2011).
- [12] D. Moody & J. Trauger, Design and demonstration of hybrid Lyot coronagraph masks for improved spectral bandwidth and throughput, *Proc. SPIE* 7010, 70103P-1 (2008).